



**HAL**  
open science

# A local electrochemical impedance study of the self-healing properties of waterborne coatings on 2024 aluminium alloy

Anh Son Nguyen, Nadine Pébère

► **To cite this version:**

Anh Son Nguyen, Nadine Pébère. A local electrochemical impedance study of the self-healing properties of waterborne coatings on 2024 aluminium alloy. *Electrochimica Acta*, 2016, 222, pp.1806-1817. 10.1016/j.electacta.2016.11.152 . hal-02433728

**HAL Id: hal-02433728**

**<https://hal.science/hal-02433728>**

Submitted on 9 Jan 2020

**HAL** is a multi-disciplinary open access archive for the deposit and dissemination of scientific research documents, whether they are published or not. The documents may come from teaching and research institutions in France or abroad, or from public or private research centers.

L'archive ouverte pluridisciplinaire **HAL**, est destinée au dépôt et à la diffusion de documents scientifiques de niveau recherche, publiés ou non, émanant des établissements d'enseignement et de recherche français ou étrangers, des laboratoires publics ou privés.



## Open Archive Toulouse Archive Ouverte (OATAO)

OATAO is an open access repository that collects the work of Toulouse researchers and makes it freely available over the web where possible

This is an author's version published in: <http://oatao.univ-toulouse.fr/24454>

**Official URL:** <https://doi.org/10.1016/j.electacta.2016.11.152>

### To cite this version:

Nguyen, Anh Son  and Pébère, Nadine  *A local electrochemical impedance study of the self-healing properties of waterborne coatings on 2024 aluminium alloy.* (2016) *Electrochimica Acta*, 222. 1806-1817. ISSN 0013-4686

Any correspondence concerning this service should be sent to the repository administrator: [tech-oatao@listes-diff.inp-toulouse.fr](mailto:tech-oatao@listes-diff.inp-toulouse.fr)

# A local electrochemical impedance study of the self-healing properties of waterborne coatings on 2024 aluminium alloy

Anh Son Nguyen<sup>a,b</sup>, Nadine Pébère<sup>a,\*</sup>

<sup>a</sup> Université de Toulouse, CIRIMAT, UPS/INPT/CNRS, ENSIACET, 4 Allée Emile Monso, CS 44362, 31030 Toulouse, France

<sup>b</sup> Laboratory for Protective Coatings, Institute for Tropical Technology, VAST, 18, Hoang Quoc Viet, Hanoi, Vietnam

## ARTICLE INFO

**Keywords:**  
aluminium alloy  
corrosion protection  
organic paints  
chromates  
self-healing

## ABSTRACT

In the present work the processes involved in the degradation of a coated 2024 aluminium alloy from an artificial scratch were investigated by local electrochemical impedance spectroscopy (LEIS). The aim was to assess the self healing process linked to the release of inhibitive pigments from the coatings. A comparison is provided for the local behaviour of a chromated coating, currently used in the aeronautic industry, and a Cr free system. Local impedance diagrams were obtained above the scratched areas for different exposure times to the electrolyte (1 mM NaCl). For the chromated sample, the impedance values were high and increased with time, clearly showing a significant inhibition in the scratch. In contrast, for the Cr free coating, impedance values were lower and in several areas, corrosion products appeared in the scratch. In these corroded zones, after several days of immersion, the diagrams have similar shape as that observed on bare 2024 aluminium alloy. Mappings, performed at 3 Hz, for different exposure times to the electrolyte also clearly showed the self healing process in the presence of chromates or the development of the corrosion for the unchromated coating. At 1 kHz, similar mappings were observed for the two systems providing support to the fact that the coatings presented good adhesion to the substrate. It must be emphasized that LEIS gives a fast response on the efficacy of the inhibitive pigments and thus, complements the information obtained from the conventional EIS technique.

## 1. Introduction

The organic coatings currently used in the aeronautic industry present very high corrosion protection. However, since the beginning of the 1990s, the high toxicity associated with hexavalent chromium, used as inhibitive pigment, has imposed restrictions on their use in industrial applications. Today, the development of new Cr free healing systems remains an important challenge because, on the one hand, the new protective systems must match the environmental regulations and on the other hand, their performances, particularly in the long term, must be preserved. During the last decades, numerous works were devoted to the development and to the assessment of new materials for corrosion protection of metallic structures including various methodologies for the incorporation of “green” corrosion inhibitors in the coatings to provide an active corrosion protection [1,2].

Starting from these considerations, we developed a wide study to obtain a better knowledge of degradation mechanisms as a function of exposure time of chromate free coatings for corrosion protection of 2024 aluminium alloy (AA2024). In a first part, commercial water based coatings formulated with either strontium chromate ( $\text{SrCrO}_4$ ) or a mixture of Cr(VI) free pigments have been compared in an impedance study [3,4]. These previous works have been focussed on the use of different models for analysing the conventional impedance data. In the present work, local electrochemical impedance measurements were performed in the presence of an artificial defect to characterize the processes involved in the degradation of the coated AA2024 and to evaluate the healing efficiency.

During the last decades, it has been demonstrated that local electrochemical impedance spectroscopy (LEIS) is a powerful tool to investigate corrosion processes on bare metal surfaces [5–14] or on coated alloys [15–28]. For instance, local impedance diagrams obtained on an AZ91 magnesium alloy have shown that it was possible to show the contribution of each phase constituting the alloy in its corrosion behaviour [8]. The LEIS technique was also used to investigate galvanic couplings, such as aluminium/copper

\* Corresponding author. Tel.: 00 33 5 34 32 34 23; fax: 00 33 5 34 32 34 99.  
E-mail address: Nadine.Peber@ensiacet.fr (N. Pébère).

[9,10] aluminium/magnesium [11] or zinc/carbon steel [12]. The Al/Cu couple was first designed by Jorcin et al. [9] to study corrosion phenomena associated with copper rich intermetallic particles in aluminium alloys. Local impedance measurements were also performed on the Al/Cu couple to analyse the role of different inhibitors on the galvanic coupling [13,14]. For example, it was shown that the galvanic coupling was strongly limited by mixing 8 hydroxyquinoline and benzotriazole which was not the case when the inhibitors were used separately [14]. Inductive loops, consistently observed on the local impedance diagrams during galvanic couplings, were attributed to the local ohmic impedance [10]. Several works were dedicated to the use of the LEIS technique to investigate the degradation of organic coatings [15–21]. As an example, Philippe et al. [21] investigated polymer coated galvanized steel. They showed that the global impedance measurements provided surface averaged responses corresponding to both the polymer properties and its defects, whereas LEIS allowed coating defects to be isolated. Jorcin et al. [22] have investigated the initiation and propagation of delamination at the steel/epoxy vinyl coating interface from an artificial defect after aging in a salt spray chamber. LEI mappings, performed at 5 kHz, revealed weak zones with poor adherence to the metal substrate around the scratches. The mappings, obtained for various exposure times to the salt spray, allowed the delamination surface area to be quantified. Macedo et al. [24] have used both global and local impedances to investigate different coatings (epoxy, alkyd and polyurethane) on a carbon steel. They showed that the anomalous increase in resistance with immersion time of the alkyd paint was linked to the nature of the polymeric network and not to phenomena occurring at the metal/paint interface. Mouanga et al. [25] have investigated a Zn Ni + chromate conversion coating deposited on carbon steel. In the presence of a large scratch (2 mm), they showed by LEIS that, after 21 days of immersion in the corrosive solution, the impedance modulus measured at 1 Hz was higher at the centre of the defect than on the coating, showing the high protection afforded by the chromate conversion coating. Recently, LEIS was used to investigate self healing ability of various inhibitors, such as 8 HQ [26–28], cerium acetylacetonate, or sodium molybdate [28] encapsulated in reservoirs and added to epoxy coatings applied on AA2024. LEIS was used in mapping mode only, at a frequency of 10 Hz, with a scanned area including a defect. The measurements carried out for different immersion times provided information on the kinetics of local inhibition by the encapsulated inhibitors in the damaged areas.

The aim of the present work is to highlight the great potential of the local impedance technique for the characterization of the self healing processes of organic coatings artificially damaged and to propose a methodology for investigating coatings containing environmentally friendly inhibitors. For this purpose, the two water based systems (chromated (CC) and unchromated (NCC)) previously characterized by conventional EIS were used [3,4]. First, local impedance measurements were performed over the scratches for various exposure times to the corrosive solution. Then, local mappings were obtained above and around the scratch at different frequencies (1 kHz, 30 Hz and 3 Hz) and for different immersion times. For the chromated system only, the influence of the width of the scratch was investigated. The results obtained with the conventional EIS [3,4] were also briefly recalled to emphasize the complementarity of global and local impedance measurements to assess the corrosion protection performance of organic coatings.

## 2. Experimental

The coating samples used and the global and local impedance measurement protocols are presented in this section.

### 2.1. Coating samples

Both CC and NCC consisted of a two component water based paint, manufactured by Mapaero SAS, Pamiers, France, using a polyaminoamide (Versamid<sup>®</sup> type) as base and a bisphenol A epoxy polymer as hardener, titanium oxide (12 wt. %), talc (11 wt. %) and silica (1 wt. %). In the CC, SrCrO<sub>4</sub> (16 wt. %) was added as inhibitive pigment, whereas in the NCC, SrCrO<sub>4</sub> was replaced by a mixture of zinc oxide and a phosphosilicate (10 wt. %). The coatings were deposited onto 2024 T3 aluminium alloy plates. The chemical composition in weight percent of the alloy was: Cu: 4.90; Mg: 1.31; Mn: 0.56; Si: 0.08; Fe: 0.26; Zn: 0.10; Ti: 0.01 and Al to balance. The specimens consisted of 125 mm × 80 mm × 1 mm plates machined from a rolled plate. Before painting, the samples were degreased at 60 °C (pH=9) for 15 min, rinsed twice with distilled water, then etched in an acid bath at 52 °C for 10 min, and rinsed again with distilled water. The liquid paints were applied by air spraying. After curing at 60 °C, the coatings were 20 ± 2 μm thick.

For most of the experiments, scratches were done manually using a cutting knife. Three scratches of 30 mm length were performed on each sample. Each scratch was observed with an optical microscope before the electrochemical measurements to check the width of the scratch and to verify that the scratch reached the substrate. The scribe has a U shape profile and was approximately 110 μm width and 100 μm depth (Fig. 1a). Some measurements were also performed, for the CC sample only, on a wider scratch (1 mm width and 200 μm depth) by using a scribing machine (Fig. 1b). The scratch size remains a relevant parameter to investigate self healing processes because mass transport of the inhibitive pigments from the coating (release step) to the freshly exposed substrate is a determining step [29], particularly when the inhibitor release is slow. For the tested chromated system, the amount of chromate release from the intact coating was previously determined by UV vis spectroscopy [4]. It can be assumed that the

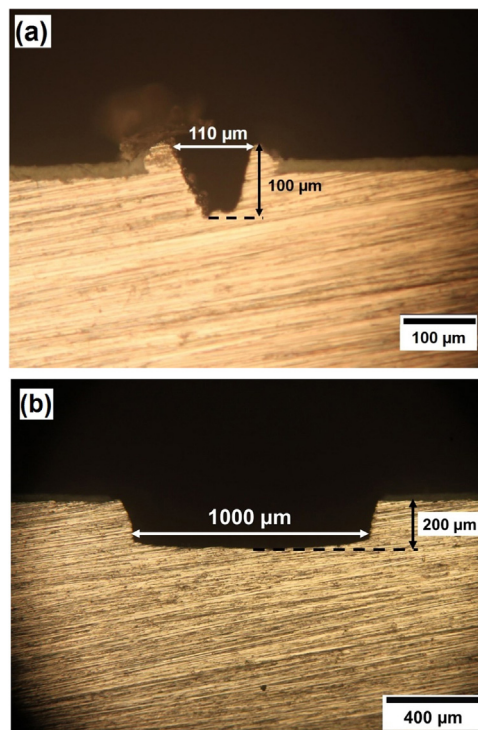


Fig. 1. Optical micrographs of the cross-section of the two types of artificial defects: (a) cutter scribing and (b) machine scribing.

leaching rate of chromate in the solution would be lower in the presence of a scratch than for the intact coating due to the chromates interaction with the AA2024 substrate (corrosion inhibition in the scratch). Moreover, the release of chromates should be dependent on the scratch size. This point was not investigated in the present study. For the Cr(VI) free pigments, it was checked that they are little soluble in the NaCl solution.

The corrosive medium was prepared from deionized water by adding NaCl (reagent grade). The concentration for the conventional impedance was 0.5 M ( $0.01 \text{ S cm}^{-1}$ ) and 1 mM ( $100 \mu\text{S cm}^{-1}$ ) for the local impedance. By decreasing the electrolyte conductivity, accurate measurements at low frequencies can be achieved [30] which is necessary to investigate the self healing processes. In the present study, a good accuracy was obtained for frequency up to 1 Hz.

## 2.2. Electrochemical impedance measurements

Global impedance measurements were performed for intact coatings in a classical three electrode cell, realized by fixing a cylindrical Plexiglas tube on top of the coated sample. The working electrode was a  $24 \text{ cm}^2$  portion of the sample. A saturated calomel electrode (SCE) and a Pt sheet were used as reference and counter electrode, respectively. A Biologic VSP apparatus was used to measure the impedance of the coated samples, for exposure times ranging from 2 hours to ca. 1 month. Measurements were performed under potentiostatic conditions, at the open circuit potential, with a 30 mV peak to peak sinusoidal perturbation. Frequency was swept downwards from  $10^5 \text{ Hz}$  to 0.01 Hz, recording 8 points per decade.

For the local electrochemical impedance measurements, a five electrode configuration was used: the scratched coated samples as working electrode, a carbon composite (Goodfellow) circular grid was used as a counter electrode, the saturated calomel electrode as a reference electrode and the bi electrode with the two platinum probes. LEIS measurements were carried out with a PAR Model 370 Scanning Electrochemical Workstation that consisted of a 370 scanning control unit, a Solartron 1287 potentiostat, a Solartron 1255 B frequency response analyser, a high impedance input amplifier using a differential electrometer, and a probe scanning assembly driven in the x, y, and z directions. LEIS measurements were performed under potentiostatic regulation, at the open circuit potential. Local impedance spectra were acquired at various locations over the scratches to verify the reproducibility. At least five measurements were performed in each scratch. The distance of the bi electrode to the working electrode was carefully controlled and the position was the same for all the experiments ( $200 \mu\text{m} \pm 50 \mu\text{m}$ ). It was checked that the distance between the probe and the substrate ( $100 \mu\text{m}$  to  $300 \mu\text{m}$ ) little affected the local impedance results. For the commercial device, the distance of the probe to the working electrode is not the main parameter because this distance is much lower than the distance between the two platinum probes (2 mm) and thus, the size of the probe (electrode dimension and inter electrode distance) is the most relevant factor which control the accuracy of the measurements and particularly limits the spatial resolution of the technique. The error on the impedance or admittance linked to the probe distance can be considered small and thus CC and NCC results can be directly compared.

The applied potential amplitude was 100 mV and the frequencies ranged from 65 kHz to 1 Hz with 8 points per decade. For the LEI mappings (LEIM), the probe was stepped across a designed area of the sample. In the present study, the analysed part was an area of  $16 \times 16 \text{ mm}$ , above and around the scratch. The step size was  $500 \mu\text{m}$  in the x and  $500 \mu\text{m}$  in the y directions. The local mappings (2D or 3D) consisted in plotting the admittance rather than the

impedance because corrosion sites are easily observable with peaks instead of valleys [17]. A relatively good reproducibility of the results was observed in the present work and the results shown for a single coating were typical of other nominally identical coatings.

## 2.3. Scanning electron microscopy (SEM) observations

SEM analyses were carried out on a LEO 435VP instrument equipped with an electron dispersive X ray (EDX) spectrometer. The accelerating voltage was 15 kV. Observations and analysis of the corrosion products formed in the scratch of the NCC sample after one month exposure to the NaCl 1 mM were performed.

## 3. Results and discussion

### 3.1. Global impedance

The results from the conventional impedance for the two coatings (CC and NCC) without defects were already published [3,4] and are briefly recalled here for a better understanding of the systems in the absence of defects. Fig. 2 compares the impedance diagrams of the CC and NCC coatings after 1 day and 1 month immersion in 0.5 M NaCl solution. For both coatings the impedance diagrams are little modified with exposure to the electrolyte. The data have been analysed with a model assuming an exponential variation of the coating resistivity along the coating thickness [3,4].

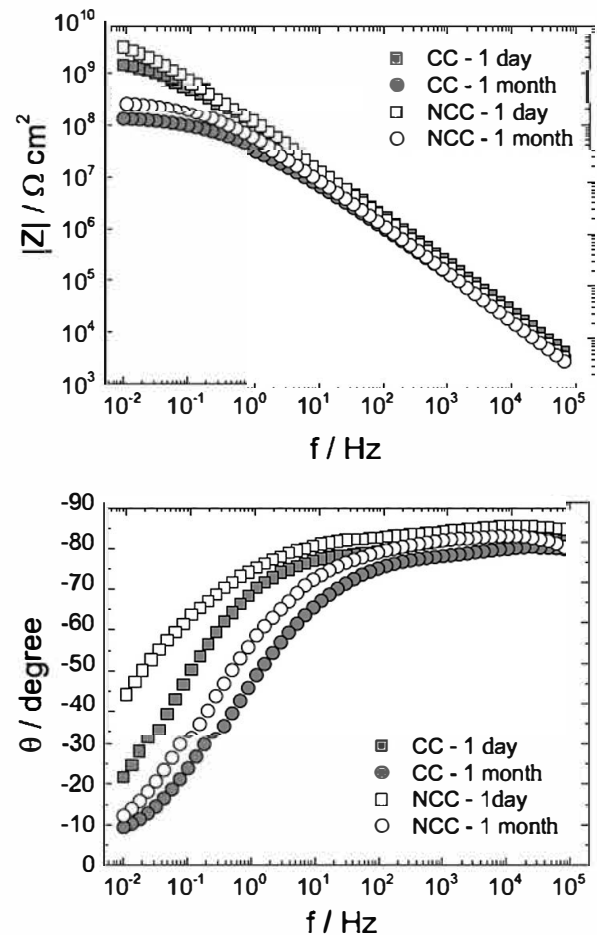


Fig. 2. Global impedance response in Bode representation for the AA2024 coated samples (CC and NCC) obtained after a day and a month immersion in 0.5 M NaCl.

The analysis confirmed that penetration of water and ions occurs on different time scales [31–35]. The former process is faster and affects permittivity more strongly than resistivity; the latter is slower and affects almost exclusively resistivity. Fig. 3 shows the variation of the impedance modulus at  $f = 10$  mHz ( $Z_{10\text{mHz}}$ ) as a function of immersion time in 0.5 M NaCl for CC and NCC. The two curves are close. It can be seen that, at the beginning of immersion, the impedance modulus is the same for the two systems and then, for both samples, it decreases when the immersion time increases. The impedance modulus is always lower for CC than for NCC which was ascribed to the leaching of chromates, and was confirmed by chemical analysis of the solution [4]. The curves in Fig. 3 are close to the curves obtained from the model showing the immersion time dependence of the zero frequency limit of the impedance ( $Z_{\text{total}}$ ) of CC and NCC (Fig. 12 in reference [4]). It is interesting to recall that although the global impedances of CC and NCC coatings were rather similar, the data analysis has shown that  $R_{\text{pore}}$  values were ten times larger for CC than for NCC and the Young impedance was initially larger but decreased at a higher rate for CC than for NCC to become ca. 10 times lower after one month [4]. Thus, it can be concluded that the global impedance diagrams mainly account for the barrier properties of the coatings. The difference between the two coatings has been attributed to chromate leaching. Finally, after 1 month immersion, the barrier properties of both coatings remained high and the AA2024 substrate was not corroded. Thus, independently of the type of pigments in the formulation, the paint durability cannot be evaluated from the global impedance results only.

### 3.2. Local impedance

#### 3.2.1. Variation of $E_{\text{corr}}$ versus exposure time in 1 mM NaCl solution

Fig. 4 shows the variation of the corrosion potential ( $E_{\text{corr}}$ ) for the CC and NCC scratched samples as a function of the exposure time to 1 mM NaCl solution. It can be seen that, from the beginning of immersion, the values are significantly different for the two samples but they remain relatively constant when the immersion time increases. For CC,  $E_{\text{corr}}$  is about 0.35 V more cathodic than for the NCC. For the intact coatings,  $E_{\text{corr}}$  was also more negative for CC than for NCC of about 0.1 V [4]. The shift of  $E_{\text{corr}}$  in the cathodic direction accounts for the inhibitive action of chromates on the corrosion of the AA2024 [36–41]. Independent polarisation curves carried out on bare AA2024 in the presence of chromates also showed a shift of  $E_{\text{corr}}$  as well as a decrease of both the anodic and

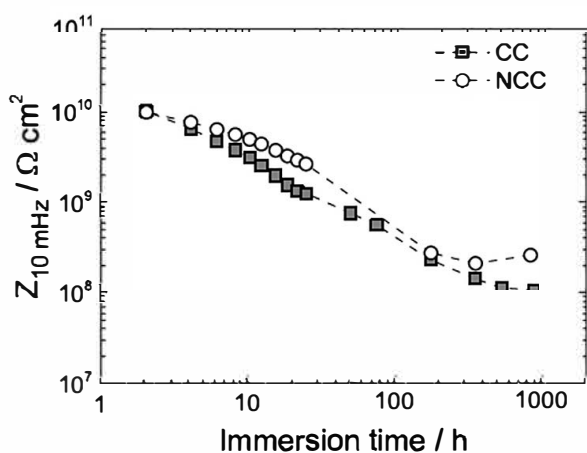


Fig. 3. Impedance modulus at 10 mHz ( $Z_{10\text{mHz}}$ ) as a function of immersion time in 0.5 M NaCl for the AA2024 samples protected by CC and NCC.

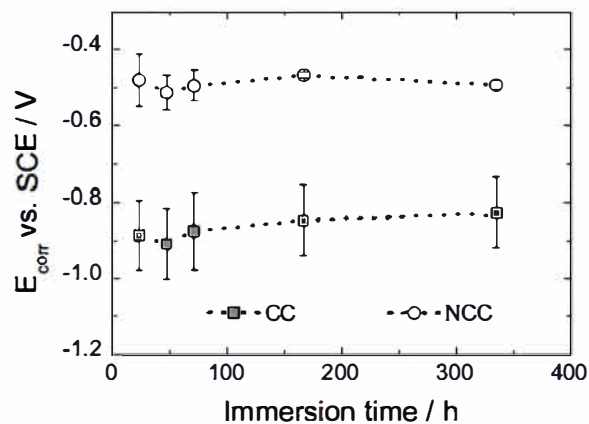


Fig. 4. Corrosion potential ( $E_{\text{corr}}$ ) as a function of immersion time in 1 mM NaCl for the scratched coated samples (small scratch). Error bars account for experiments performed on two samples and five scratches.

cathodic current densities (not shown). Here, the significant shift of  $E_{\text{corr}}$  for the CC sample confirmed the inhibitive action of chromates which strongly limited the oxygen reduction reaction on the intermetallic particles of the AA2024 and improves the oxide film formation. For the wider scratch (1 mm),  $E_{\text{corr}}$  was about  $-0.6$  V/SCE instead of  $-0.9$  V/SCE for the narrow scratch. This difference would be linked to the chromates content in the scratch and would suggest that the specific action of chromates on the cathodic sites (intermetallic particles) and/or anodic sites (aluminium matrix) would be dependent on their concentration. For the CC sample, the scratches remained bright even after several months of immersion. This indicates that the release of chromates from the coating was enough to prevent corrosion.

#### 3.2.2. Influence of the immersion time

To verify the reproducibility of the measurements, several local impedance diagrams were acquired at various locations over the scratches. As an example, six different measurements obtained on CC and NCC samples are shown in Fig. 5. For the CC sample, the diagrams are almost superimposed accounting for a good reproducibility (Fig. 5a and b). Instead, for the NCC the diagrams are not strictly identical. As it will be discussed later, corrosion appeared in the scratches but only in some areas and thus, a larger variability of the impedance response was observed (Fig. 5c and 5d). All the diagrams (CC and NCC) presented the same shape in the high frequency range ( $f > 1$  kHz) with the presence of an additional time constant attributed to local Ohmic impedance [10,30]. The high frequency part of the diagrams will not be discussed for the remainder of the study. For CC, some points at low frequency, around 1 Hz, are scattered (Fig. 5b). This indicates that, in our configuration, the highest value of the local impedance which can be accurately measured is around  $10^6 \Omega \text{ cm}^2$  [30].

Fig. 6 shows the impedance diagrams (Nyquist and Bode representations) for CC obtained over the scratch for different immersion times. A capacitive behaviour with high impedance values can be observed independently of the immersion time. Moreover, the impedance modulus increases until 336 h of immersion and then stabilizes. These observations confirmed the corrosion inhibition of AA2024 in the scratch and the progressive formation of a protective layer. For the NCC, two different zones were observed, particularly visible after 24 h of immersion: one with a black deposit and another one with white corrosion products. SEM observations and EDX analysis were performed in the scratch of the NCC sample after one month of

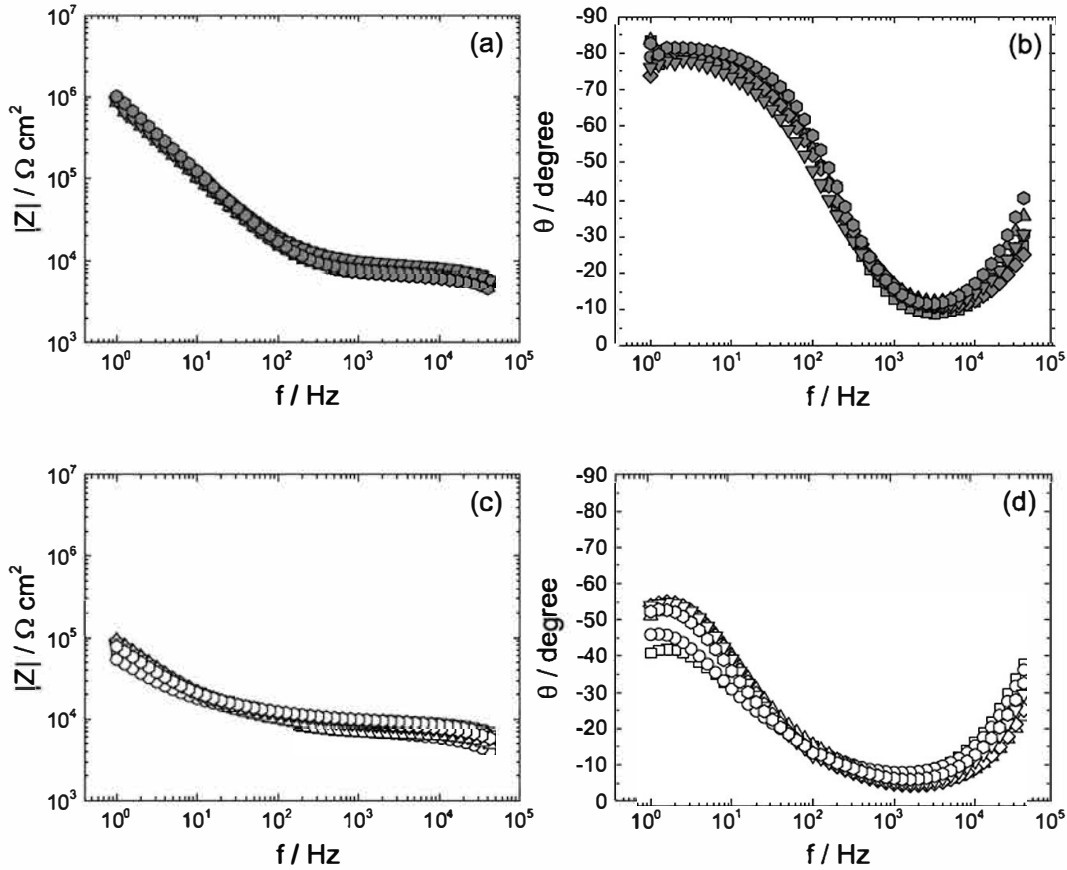


Fig. 5. Local impedance diagrams (Bode coordinates) obtained over the scratches after 24h immersion in 1 mM NaCl: (a, b) CC and (c, d) NCC – results of six independent measurements are shown on the figures: (a, c) modulus and (b, d) phase angle.

exposure to the 1 mM NaCl solution (Fig. 7). The EDX spectrum of the black deposit (Fig. 7a) revealed the presence of Si, S and Zn which would indicate the presence of zinc oxide and phospho silicate, incorporated in the coating to replace chromates. In the corroded area (Fig. 7b), the Al, Cu and Mg peaks, characterizing the  $Al_2CuMg$  particles, can clearly be seen and the Si, S and Zn peaks are not observed, in agreement with the development of the corrosion. The local impedance diagrams recorded above these two areas display different behaviours (Fig. 8). The diagrams are characterized by a single capacitive loop but the impedance values are about ten times lower on the corroded zone. Over the black deposit, the impedance slightly increases with immersion time (Fig. 8a) but over the corroded area, the impedance decreases (Fig. 8b). Fig. 9 compares the local impedance diagrams in Bode coordinates obtained for the two distinct areas of the NCC sample after 24 h and 504 h of immersion. The diagram of the bare AA2024 is reported in Fig. 9 for comparison. In the presence of the black deposit, the impedance modulus slightly increases between 24 h and 504 h immersion (from  $1 \times 10^5$  to  $5 \times 10^5 \Omega \text{ cm}^2$ ) which would be indicative of a protective action of the deposit. On the corroded area, the shape of the diagram after 24 h of immersion is similar to that obtained on the black deposit for the same immersion time except a slightly lower impedance modulus. After 504 h of immersion, the impedance modulus on the corroded zone decreases (from  $6 \times 10^4$  to  $2 \times 10^4 \Omega \text{ cm}^2$ ) and the diagram is close to that obtained on the bare AA2024, showing that the substrate was not protected in this area.

From the local impedance diagrams obtained for both CC and NCC, three parameters were graphically extracted: the impedance

modulus at low frequency ( $Z_{1Hz}$ ), the parameters  $\alpha$  and  $Q$ , associated to a constant phase element (CPE) which account for the non ideal behaviour of the systems. For CC, the  $\alpha$  and  $Q$  values were graphically determined with a good accuracy in a large frequency range [42]. For the NCC, on the corroded areas, the parameters  $\alpha$  and  $Q$  cannot be accurately measured and, for this reason, are not reported in Fig. 10 which shows the variation of the parameters as a function of immersion time in 1 mM NaCl solution. For CC, the values of  $Z_{1Hz}$  increase during the first days of immersion, until 72 h and then, remain stable around  $2 \times 10^6 \Omega \text{ cm}^2$  for longer immersion times (Fig. 10a). For the NCC, the impedance modulus are lower than for the CC. For short immersion times, whether in presence of the black deposit or the corrosion products in the scratch, the values of  $Z_{1Hz}$  are comparable but ten times lower than those obtained over the scratch for CC. When the immersion time increases, while the impedance modulus remains constant above the black deposit, it progressively decreases on the corroded area. For the NCC, these results can be explained by the fact that, at the beginning of immersion, the black deposit was formed all along the scratch and the impedance modulus was the same independently of the analysed area. When the immersion time increases, the corrosion starts at some locations and the modulus decreased. The self healing process or the corrosion growth can be also observed on the variation of the CPE parameters. For the CC, the parameter  $\alpha$  is independent of the immersion time and is around 0.9 (Fig. 10b). The values of  $Q$  are low ( $10^{-7} \Omega^{-1} \text{ cm}^{-2} \text{ s}^\alpha$ ) and characterize a film effect rather than a double layer capacitance. The parameter  $Q$  slightly decreases when the immersion time increases (Fig. 10c). This behaviour, in

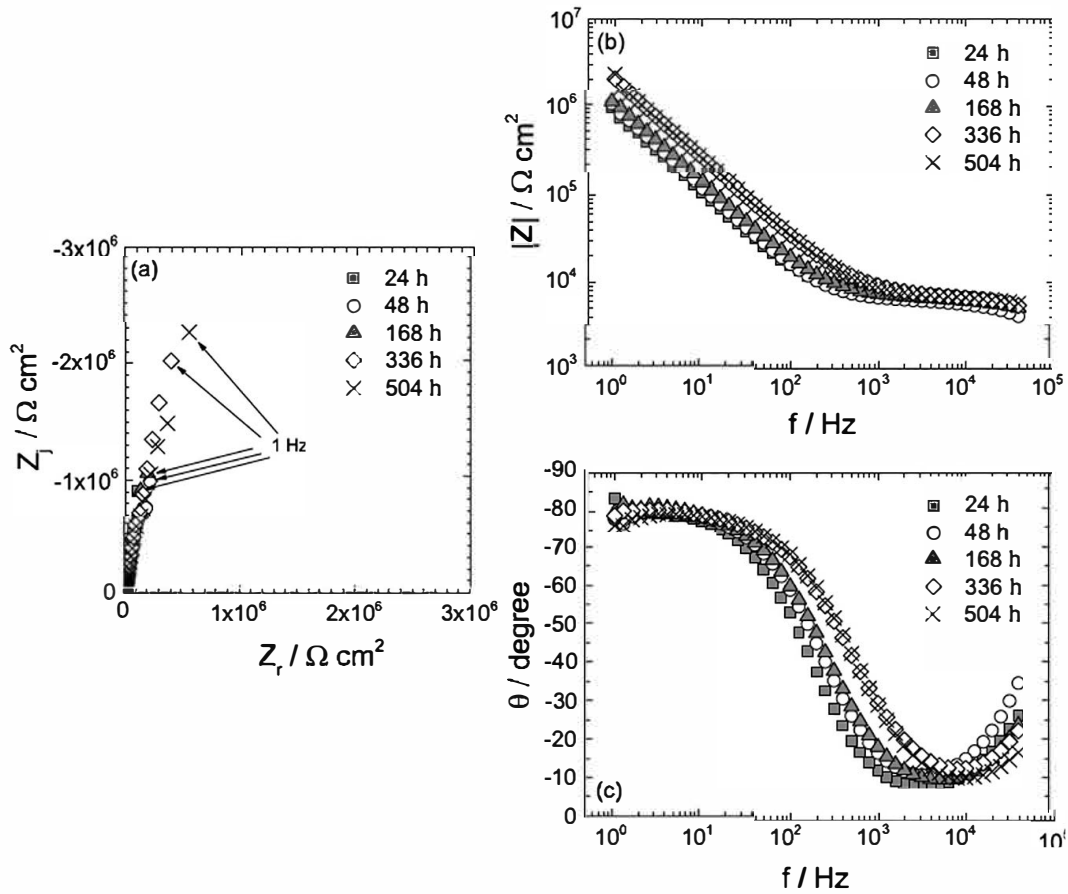


Fig. 6. Local impedance diagrams above the scratch for CC as a function of immersion time in 1 mM NaCl: (a) Nyquist, (b) impedance modulus and (c) phase angle.

agreement with the increase of  $Z_{1\text{Hz}}$ , would be linked to the reinforcement of the protective properties of the oxide film by the chromates [36–41]. For the NCC, the  $\alpha$  value increases with time (from 0.6 for 24 h to 0.8 after 336 h of immersion), but the value is always lower than that obtained for the CC (Fig. 10b). The values of  $Q$  for the NCC decrease when the immersion time increases

(Fig. 10c) and are ten times higher than for the CC. In this case,  $Q$  values are in the order of magnitude of a double layer capacitance. From these results, it can be concluded that for the NCC, there is no long term protection even though the presence of black deposit limits the development of the corrosion at the beginning of the exposure to the electrolyte.

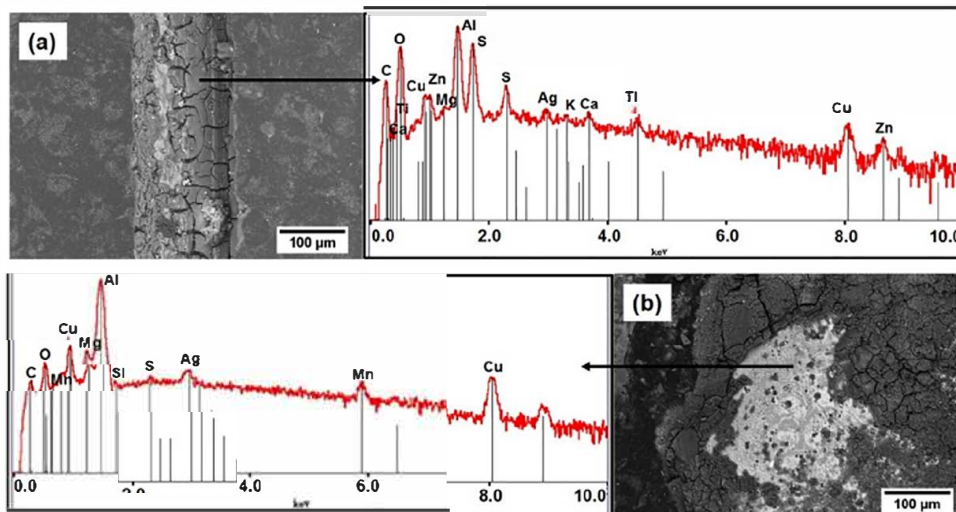


Fig. 7. SEM images and EDX analysis performed on the scratched area of the NCC sample after one month of immersion in 1 mM NaCl: (a) black deposit (b) corroded area.

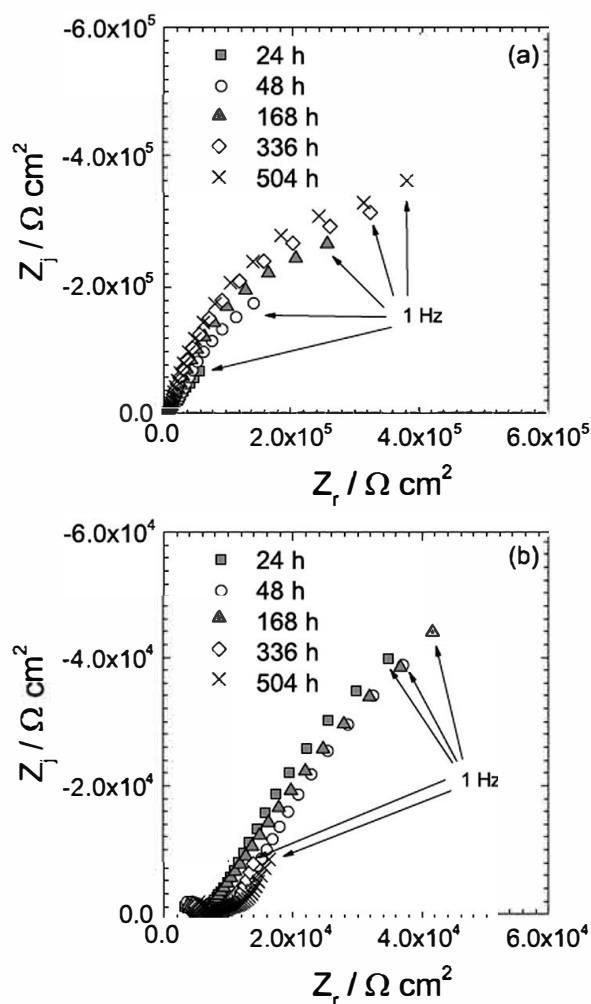


Fig. 8. Local impedance diagrams (Nyquist representation) obtained for NCC at two different locations over the scratch as a function of immersion time in 1 mM NaCl: (a) non-corroded zone and (b) corroded zone.

### 3.2.3. Mappings of the scratched samples

When using the local impedance technique, it is interesting to map the sample surface around the scratched area. The choice of the frequency to perform the mapping is a relevant parameter. Fig. 11 shows the admittance modulus over the scratch for CC and NCC after 504 h of exposure to 1 mM NaCl. The curves obtained after 24 h of immersion for the bare AA2024 and the intact coating are reported for comparison in Fig. 11. In the HF range ( $f > 1$  kHz), the curves account for the ohmic drop and for the current and potential distributions [10,30]. Around 1 kHz, the admittance modulus on the scratched samples (CC and NCC) are relatively close but when the frequency decreases, clear differences can be observed between the samples. Particularly at low frequency ( $f = 1$  Hz), the admittance value measured above the corroded area for NCC is close to that obtained for the bare AA2024 but in contrast, the admittance value obtained above the scratch for the CC sample is of the same order of magnitude to that obtained for the intact coating. This figure underlined that, depending on the frequency used to map the surface, different phenomena might be observed.

Fig. 12 presents some mappings (3D) performed over the scratched area for three frequencies (1 kHz, 30 Hz and 3 Hz) for the CC and NCC samples after 1 month of exposure to 1 mM NaCl. At 1 kHz, the mappings for the two systems are identical and the

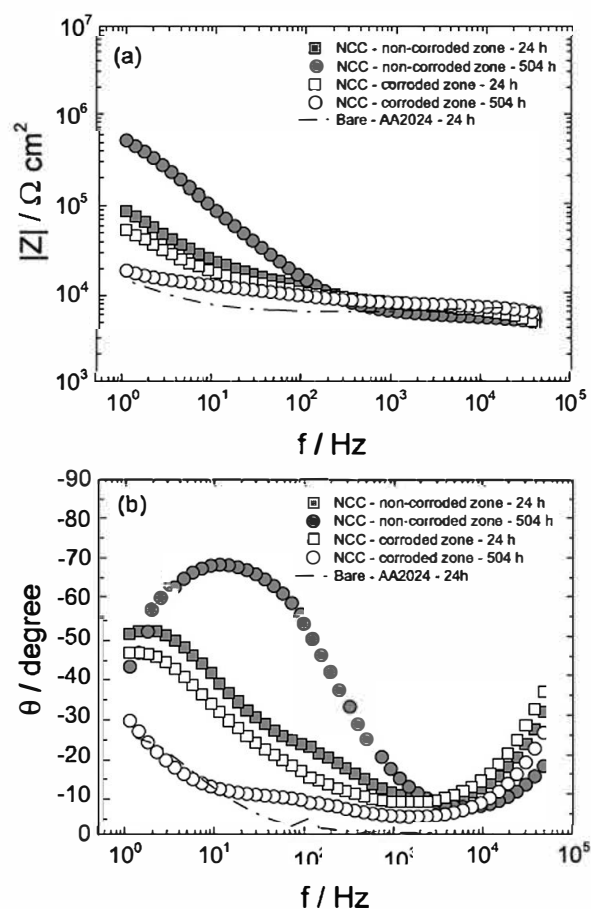


Fig. 9. Local impedance diagrams (Bode representation) obtained for NCC after 24 h and 504 h of immersion in 1 mM NaCl at two different locations above the scratch: non-corroded zone (open symbol) and corroded zone (solid symbol).

scratch is clearly visible (Fig. 12a and d). It can be emphasized that, even after one month of immersion in the electrolyte, there is no admittance step observable on the edge of the scratch, which could be attributed to coating delamination [22]. This result would indicate that the adhesion of the coatings is high, independently of the types of pigments used in the formulation. The good adhesion would be mainly linked to the chemical composition of the coating and to the surface pre treatment. At 30 Hz and 3 Hz, the mappings show that the admittance values in the scratch for CC (Fig. 12b and c) are lower than those measured for NCC (Fig. 12e and f). For NCC, the corroded and non corroded zones can be easily observed, particularly at 3 Hz, where the two zones are well separated (two peaks can be seen on the mapping which correspond to the areas with corrosion products (Fig. 12f)). At 3 Hz and for CC, the admittance values in the scratch are of the same order of magnitude than those measured above the coating and the scratch is no longer clearly visible on the mapping (Fig. 12c). From these data, it can be concluded, as expected, that a low frequency is appropriate to show the self healing process, in the present case, linked to the release of chromates from the coating. As example, mappings performed at 3 Hz for CC and NCC are reported in Fig. 13 for short immersion times. After 24 h of immersion, the admittance of CC sample is significantly lower than that of the NCC, showing that the self healing by the chromates is fast and effective. For CC, the admittance progressively decreases when the immersion time increases, showing the improvement of the corrosion resistance in the scratch, in agreement with the local impedance diagrams

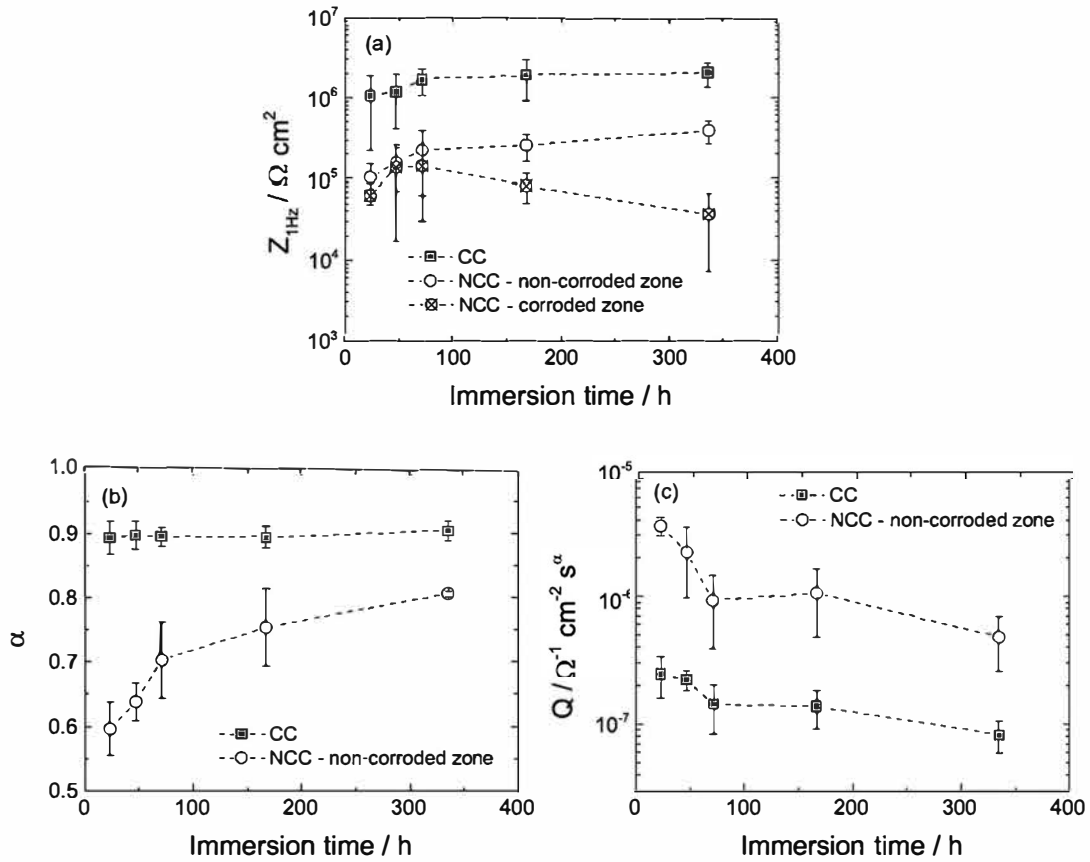


Fig. 10. Variation as a function of immersion time in 1 mM NaCl of different parameters extracted from the local impedance diagrams for CC and NCC: (a) impedance modulus at 1 Hz ( $Z_{1\text{Hz}}$ ) and (b, c) CPE parameters ( $\alpha$  and  $Q$ ). Error bars account for experiments performed on two samples and five scratches.

(Figs. 6 and 10). After 168 h of immersion, the scratch becomes almost invisible at this admittance scale (Fig. 13c). For NCC, a decrease of the admittance can be noticed between 24 h and 48 h of immersion (Fig. 13d and e) which can be explained by the presence of the dark deposit in the scratch (Fig. 7a). After 168 h of immersion

(Fig. 13f), an admittance peak is observed in the mapping, linked to the appearance of localized corrosion (Fig. 7b).

Finally, it is interesting to investigate the self healing process for the CC sample on a wider scratch. Fig. 14 shows the 2D mappings obtained above a scratch of 1 mm width. The mappings are compared to those obtained for the scratch of 110  $\mu\text{m}$  width. After 3 h of immersion, the difference in the size of the two scratches are clearly seen. In the middle of the large scratch, the admittance modulus is higher than that measured on the edge (Fig. 14d). However, on the edge, the admittance values are similar to those observed over the small scratch (Fig. 14a). For the small scratch, the mapping indicates that chromate release was sufficient to induce the self healing in the whole scratch but for the large scratch, the chromates have not yet reached the middle of the scratch which remains active. After 72 h of immersion, the self healing process is clearly visible for the small scratch, characterized by the decrease of the admittance in the scratch (Fig. 14b). In the middle of the large scratch, some areas always present high admittance values (Fig. 14e). The interesting result is that, after 168 h of immersion, the self healing process is also clearly seen on the large scratch (Fig. 14f). The strong decrease of the admittance confirms the inhibitive action of chromates and the formation of a protective layer in the scratch. After 168 h of immersion, the difference in size between the two scratches is no longer discernible on the mappings (Fig. 14c and d). These results showed that the inhibition of the corrosion of AA2024 is controlled by the release and the mass transport of chromated species from the paint to the centre of the scratch; it appeared that the chromate concentration is sufficient to protect the AA2024 surface. This analysis is in agreement with the fact that at the beginning of

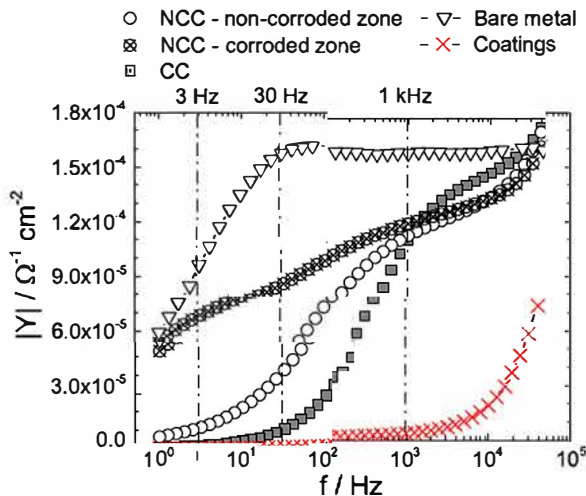


Fig. 11. Local admittance modulus obtained over the scratches for CC and NCC after 504 h of immersion in 1 mM NaCl. Comparison with the local admittance modulus of the bare AA2024 and of the intact coating.

exposure to the electrolyte, the cathodic reaction on the intermetallic particles is limited by the presence of chromates in the scratch (shift of  $E_{corr}$  in the cathodic direction (Fig. 4)). Then,

for longer exposure time, the release of chromates in the scratch progressively increased which improved the anodic passivation of the alloy surface (Fig. 6).

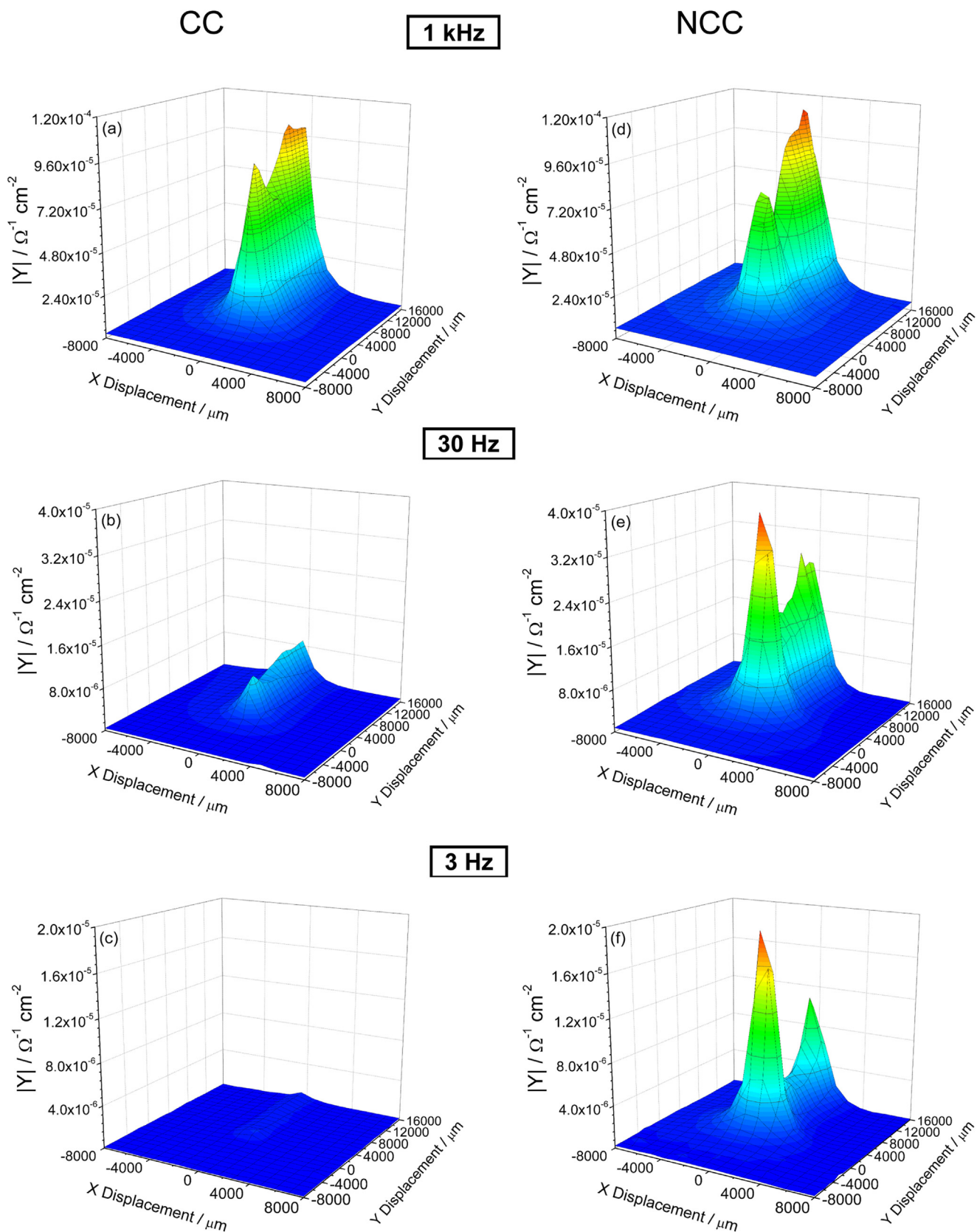
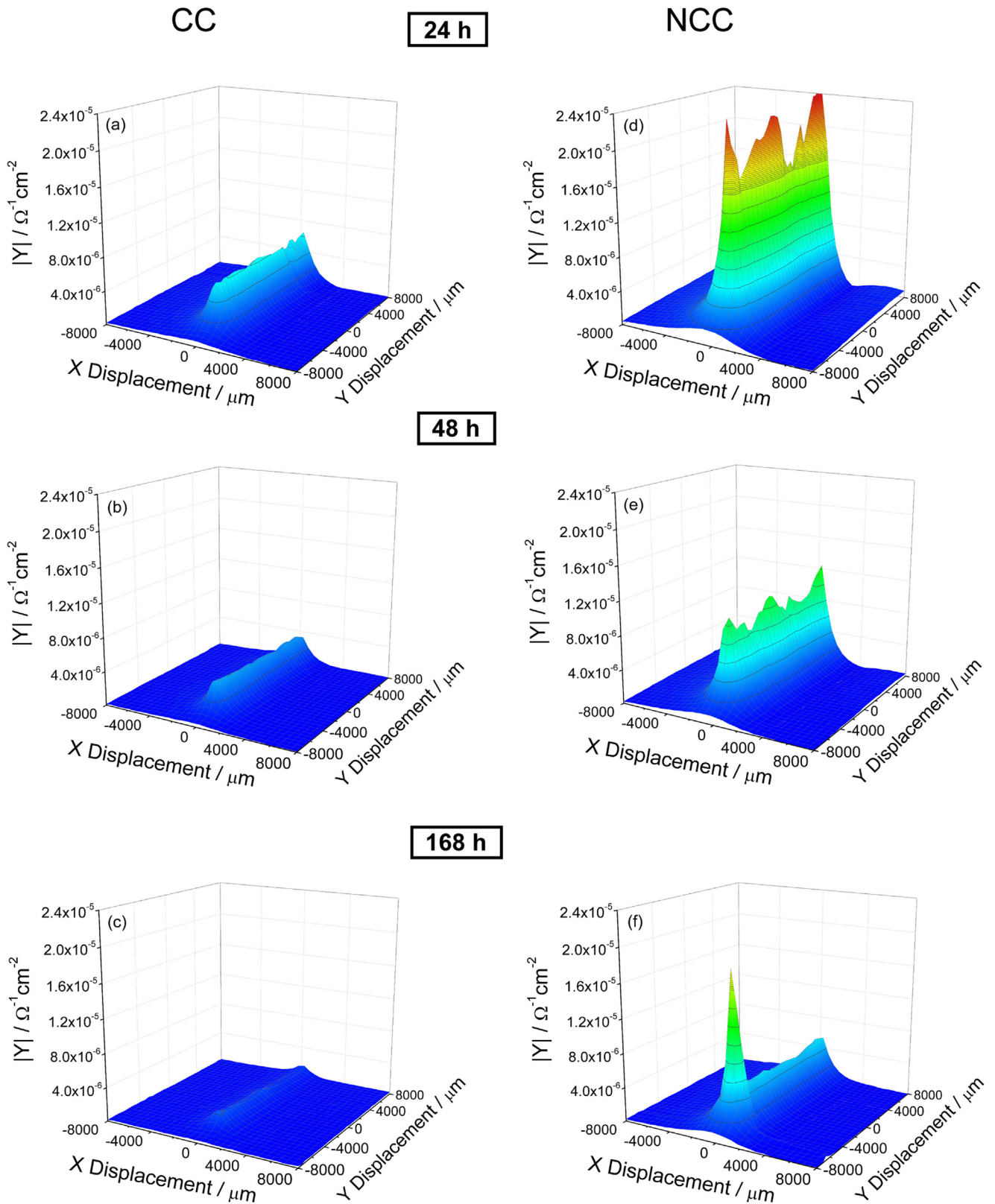
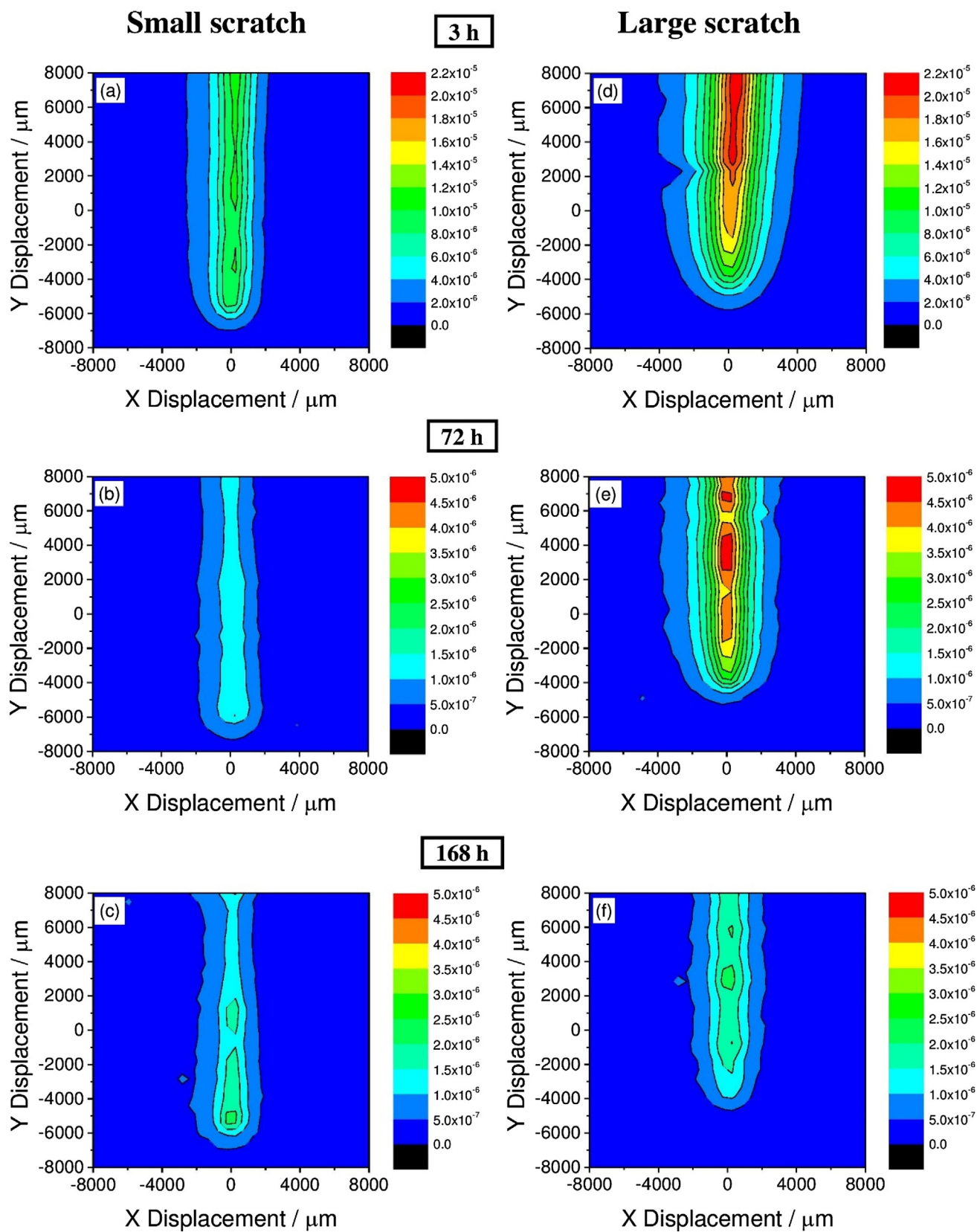


Fig. 12. Local admittance mappings performed at 1 kHz, 30 Hz and 3 Hz over the scratch for: (a, b, c) CC and (d, e, f) NCC after a month immersion in 1 mM NaCl.



**Fig. 13.** Local admittance mappings performed at 3 Hz over the scratch after 24h, 48h and 168h of immersion in 1 mM NaCl for: (a, b, c) CC and (d, e, f) NCC.



**Fig. 14.** Local admittance mappings (2D) performed at 3 Hz over the scratch after 3 h, 72 h and 168 h of immersion in 1 mM NaCl for the CC sample: (a, b, c) small scratch and (d, e, f) large scratch.

## 4. Conclusions

Local electrochemical impedance spectroscopy was used to assess the self healing process linked to the release of inhibitive pigments from the coatings. From the local impedance diagrams obtained above the scratched areas for different exposure times to the electrolyte, the self healing process was clearly observed for the chromated system. The self healing can be also observed by the mappings above the scratch at a frequency of 3 Hz. From LEIS measurements a better understanding of local corrosion inhibition mechanisms was obtained. It is interesting to point out that the mapping at 1 kHz provided support to the fact that the two systems presented good adhesion to the substrate. Finally, it can be emphasized that global and local impedances are complementary techniques to assess corrosion protection performance of organic coatings. The present work proposed a methodology (with chromates as reference) which can be used to characterize the self healing processes of coatings containing environmentally friendly inhibitors.

## Acknowledgments

The authors gratefully acknowledge the company MAPAERO (Pamiers, France) for the preparation of the coated samples and more particularly Pauline Côte and Pierre Jean Lathière for fruitful discussion on coating technologies. The PhD thesis of Nguyen Anh Son was prepared in the framework of the associated international laboratory "Functional Composite Materials (FOCOMAT)" between France and Vietnam.

## References

- [1] Handbook of smart Coatings for Material Protection, Edited by A.S.M. Makhoulouf, Woodhead Publishing Series in Metals and Surface Engineering (2014).
- [2] Smart Composite Coatings and Membranes, Transport, Structural, Environmental and Energy Applications, Edited by F. Montemor, Woodhead Publishing Series in Composites Science and Engineering (2016).
- [3] A.S. Nguyen, M. Musiani, M.E. Orazem, N. Pèbère, B. Tribollet, V. Vivier, Impedance analysis of the distributed resistivity of coatings in dry and wet conditions, *Electrochim. Acta* 179 (2015) 452.
- [4] A.S. Nguyen, M. Musiani, M.E. Orazem, N. Pèbère, B. Tribollet, V. Vivier, Impedance study of the influence of chromates on the properties of waterborne coatings deposited on 2024 aluminium alloy, *Corros. Sci.* 109 (2016) 174.
- [5] R.S. Lillard, P.J. Moran, H.S. Isaacs, A novel method for generating quantitative local electrochemical impedance spectroscopy, *J. Electrochem. Soc.* 139 (1992) 1007.
- [6] D. Zou, A High-Resolution Probe for Localized Electrochemical Impedance Spectroscopy Measurements, *J. Electrochem. Soc.* 144 (1997) 1208.
- [7] I. Annergren, D. Thierry, F. Zou, Localized Electrochemical Impedance Spectroscopy for Studying Pitting Corrosion on Stainless Steels, *J. Electrochem. Soc.* 144 (1997) 1957.
- [8] G. Galicia, N. Pèbère, B. Tribollet, V. Vivier, Local and global electrochemical impedances applied to the corrosion behaviour of an AZ91 magnesium alloy, *Corros. Sci.* 51 (2009) 1789.
- [9] J.B. Jorcin, C. Blanc, N. Pèbère, B. Tribollet, V. Vivier, Galvanic coupling between pure copper and pure aluminum: experimental approach and mathematical model, *J. Electrochem. Soc.* 155 (2008) C46.
- [10] C. Blanc, M.E. Orazem, N. Pèbère, B. Tribollet, V. Vivier, S. Wu, The origin of the complex character of the Ohmic impedance, *Electrochim. Acta* 55 (2010) 6313.
- [11] L. Lacroix, C. Blanc, N. Pèbère, B. Tribollet, V. Vivier, Localized approach to galvanic coupling in an aluminum-magnesium system, *J. Electrochem. Soc.* 156 (2009) C259.
- [12] M. Mouanga, M. Puiggali, B. Tribollet, V. Vivier, N. Pèbère, O. Devos, Galvanic corrosion between zinc and carbon steel investigated by local electrochemical impedance spectroscopy, *Electrochim. Acta* 88 (2013) 6.
- [13] G. Boisier, N. Portail, N. Pèbère, Corrosion inhibition of 2024 aluminium alloy by sodium decanoate, *Electrochim. Acta* 55 (2010) 6182.
- [14] S. Marcelin, N. Pèbère, Synergistic effect between 8-hydroxyquinoline and benzotriazole for the corrosion protection of 2024 aluminium alloy: A local electrochemical impedance approach, *Corros. Sci.* 101 (2015) 66.
- [15] R.S. Lillard, J. Kruger, W.S. Tait, P.J. Moran, Using local electrochemical impedance spectroscopy to examine coating failure, *Corrosion* 51 (1995) 251.
- [16] F. Zou, D. Thierry, Localized electrochemical impedance spectroscopy for studying the degradation of organic coatings, *Electrochim. Acta* 42 (1997) 3293.
- [17] M.W. Wittmann, R.B. Leggat, S.R. Taylor, The Detection and Mapping of Defects in Organic Coatings Using Local Electrochemical Impedance Methods, *J. Electrochem. Soc.* 146 (1999) 4071.
- [18] A.M. Mierisch, J. Yuan, R.G. Kelly, S.R. Taylor, Probing Coating Degradation on AA2024-T3 Using Local Electrochemical and Chemical Techniques, *J. Electrochem. Soc.* 146 (1999) 4449.
- [19] S.R. Taylor, Incentives for using local electrochemical impedance methods in the investigation of organic coatings, *Prog. Org. Coat.* 43 (2001) 141.
- [20] A.M. Mierisch, S.R. Taylor, Understanding the degradation of organic coatings using local electrochemical impedance methods, *J. Electrochem. Soc.* 150 (2003) B303.
- [21] L.V.S. Philippe, G.W. Walter, S.B. Lyon, Investigating localized degradation of organic coatings comparison of electrochemical impedance spectroscopy with local electrochemical impedance spectroscopy, *J. Electrochem. Soc.* 150 (2003) B111.
- [22] J.-B. Jorcin, E. Aragon, C. Merlatti, N. Pèbère, Delaminated areas beneath organic coating: a local electrochemical impedance approach, *Corros. Sci.* 48 (2006) 1779.
- [23] C. Zhong, X. Tang, Y.F. Cheng, Corrosion of steel under the defected coating studied by localized electrochemical impedance spectroscopy, *Electrochim. Acta* 53 (2008) 4740.
- [24] M. Macedo, I.C.P. Margarit-Mattos, F.L. Fragata, J.B. Jorcin, N. Pèbère, O.R. Mattos, Contribution to a better understanding of different behaviour patterns observed with organic coatings evaluated by electrochemical impedance spectroscopy, *Corros. Sci.* 51 (2009) 1322.
- [25] M. Mouanga, M. Puiggali, O. Devos, EIS and LEIS investigation of aging low carbon steel with Zn-Ni coating, *Electrochim. Acta* 106 (2013) 82.
- [26] D. Snihirova, L. Liphardt, G. Grundmeier, F. Montemor, Electrochemical study of the corrosion inhibitor ability of smart coatings applied on AA2024, *J. Solid State Electrochem.* 17 (2013) 2183.
- [27] D. Snihirova, S.V. Lamaka, M.M. Cardoso, J.A.D. Condeco, H.E.C.S. Ferreira, M.F. Montemor, pH-sensitive polymeric particles with increased inhibitor-loading capacity as smart additives for corrosion protective coatings for AA2024, *Electrochim. Acta* 145 (2014) 123.
- [28] I.A. Kartsonakis, E. Athanasopoulou, D. Snihirova, B. Martins, M.A. Koklioti, M.F. Montemor, G. Kordas, C.A. Charitidis, Multifunctional epoxy coatings combining a mixture of traps and inhibitor loaded nanocontainers for corrosion protection of AA2024-T3, *Corros. Sci.* 85 (2014) 147.
- [29] R. Oltra, F. Peltier, Influence of mass transport on the competition between corrosion and passivation by inhibitor release after coating breakdown, *Prog. Org. Coat.* 92 (2016) 44-53.
- [30] V.M.-W. Huang, S.-L. Wu, M.E. Orazem, N. Pèbère, B. Tribollet, V. Vivier, Local electrochemical impedance spectroscopy: a review and some recent developments, *Electrochim. Acta* 56 (2011) 8048.
- [31] V.B. Mišković-Stanković, D.M. Dražić, M.J. Teodorović, Electrolyte penetration through epoxy coatings electrodeposited on steel, *Corros. Sci.* 37 (1995) 241.
- [32] V.B. Mišković-Stanković, D.M. Dražić, Z. Kačarević-Popović, The sorption characteristics of epoxy coatings electrodeposited on steel during exposure to different corrosive agents, *Corros. Sci.* 38 (1996) 1513.
- [33] J.M. Hu, J.Q. Zhang, C.N. Cao, Determination of water uptake and diffusion of Cl<sup>-</sup> ion in epoxy primer on aluminum alloys in NaCl solution by electrochemical impedance spectroscopy, *Prog. Org. Coat.* 46 (2003) 273.
- [34] Q. Zhou, Y. Wang, Comparison of clear coating degradation in NaCl solution and pure water, *Prog. Org. Coat.* 76 (2013) 1674.
- [35] Y. Dong, Q. Zhou, Relationship between ion transport and the failure behaviour of epoxy resin coatings, *Corros. Sci.* 78 (2014) 22.
- [36] M.W. Kendig, A.J. Davenport, H.S. Isaacs, The mechanism of corrosion inhibition by chromate conversion coatings from x-ray absorption and near edge spectroscopy (XANES), *Corros. Sci.* 34 (1993) 41.
- [37] M. Kendig, S. Jeanjaquet, R. Addison, J. Waldrop, Role of hexavalent chromium in the inhibition of corrosion of aluminum alloys, *Surf. Coat. Technol.* 140 (2001) 58.
- [38] A. Kolics, A.S. Besing, A. Wieckowski, Interaction of Chromate Ions with Surface Intermetallics on Aluminum Alloy 2024-T3 in NaCl Solutions, *J. Electrochem. Soc.* 148 (2001) B322.
- [39] M.W. Kendig, R.G. Buccheit, Corrosion inhibition of aluminum and aluminum alloys by soluble chromates, chromate coatings and chromate-free coatings, *Corrosion* 59 (2003) 379.
- [40] S.A. Furman, F.H. Scholes, A.E. Hughes, D.N. Jamieson, C.M. Macrae, A.M. Glenn, Corrosion in artificial defects. II. Chromate reactions, *Corros. Sci.* 48 (2006) 1827.
- [41] J.D. Ramsey, R.L. McCreery, In situ Raman microscopy of chromate effects on corrosion pits in aluminum alloy, *J. Electrochem. Soc.* 146 (1999) 4076.
- [42] M.E. Orazem, N. Pèbère, B. Tribollet, Enhanced graphical representation of electrochemical impedance data, *J. Electrochem. Soc.* 153 (2006) B129.